

# Excitation of a one-dimensional evanescent wave by conical edge diffraction of surface plasmon

Johann Berthelot, Alexandre Bouhelier,\* Gérard Colas des Francs,  
Jean-Claude Weeber and Alain Dereux

Laboratoire Interdisciplinaire Carnot de Bourgogne, CNRS-UMR 5209, Université de Bourgogne, 21078 Dijon, France

[\\*alexandre.bouhelier@u-bourgogne.fr](mailto:alexandre.bouhelier@u-bourgogne.fr)

**Abstract:** The experimental observation of a one-dimensional evanescent wave supported by a  $90^\circ$  metal edge is reported. Through a measurement of in-plane momenta, we clearly demonstrate the dimensional character of this surface wave and show that it is non-radiative in the superstrate. Excitation conditions, lateral extension and polarization properties of this wave are discussed. Finally, we explore the effect of the surrounding dielectric medium and demonstrate that a single edge can sustain distinct excitations.

© 2011 Optical Society of America

**OCIS codes:** (240.0240) Optics at surfaces; (240.6680) Surface plasmons; (240.3695) Linear and nonlinear light scattering from surface; (260.6970) Total internal reflection.

---

## References and links

1. S. I. Bozhevolnyi, V. S. Volkov, E. Devaux, and T. W. Ebbesen, "Channel plasmon-polariton guiding by sub-wavelength metal grooves," *Phys. Rev. Lett.* **95**, 046802 (2005).
2. T. Yatsui, M. Kourogi, and M. Ohtsu, "Plasmon waveguide for optical far/near-field conversion," *Appl. Phys. Lett.* **79**, 4583–4585 (2001).
3. E. Moreno, S. G. Rodrigo, S. I. Bozhevolnyi, L. Martín-Moreno, and F. J. García-Vidal, "Guiding and focusing of electromagnetic fields with wedge plasmon polaritons," *Phys. Rev. Lett.* **100**, 023901 (2008).
4. J. Takahara, S. Yamagishi, H. Taki, A. Morimoto, and T. Kobayashi, "Guiding of a one-dimensional optical beam with nanometer diameter," *Opt. Lett.* **22**, 475–477 (1997).
5. H. Ditlbacher, A. Hohenau, D. Wagner, U. Kreibitz, M. Rogers, F. Hofer, F. R. Aussenegg, and J. R. Krenn, "Silver nanowires as surface plasmon resonators," *Phys. Rev. Lett.* **95**, 257403 (2005).
6. J.-C. Weeber, Y. Lacroute, and A. Dereux, "Optical near-field distributions of surface plasmon waveguide modes," *Phys. Rev. B* **68**, 115401 (2003).
7. R. Zia, J. A. Schuller, and M. L. Brongersma, "Near-field characterization of guided polariton propagation and cutoff in surface plasmon waveguides," *Phys. Rev. B* **74**, 165415 (2006).
8. R. F. Wallis, A. A. Maradudin, and G. I. Stegeman, "Surface polariton reflection and radiation at end faces," *Appl. Phys. Lett.* **42**, 764–766 (1983).
9. P. Dawson, F. de Fornel, and J.-P. Goudonnet, "Imaging of surface plasmon propagation and edge interaction using a photon scanning tunneling microscope," *Phys. Rev. Lett.* **72**, 2927–2930 (1994).
10. F. I. Baida, D. Van Labeke, and J.-M. Vigoureux, "Near-field surface plasmon microscopy: A numerical study of plasmon excitation, propagation, and edge interaction using a three-dimensional gaussian beam," *Phys. Rev. B* **60**, 7812–7815 (1999).
11. K. Hasegawa, J. U. Nöckel, and M. Deutsch, "Surface plasmon polariton propagation around bends at a metal-dielectric interface," *Appl. Phys. Lett.* **84**, 1835–1837 (2004).
12. R. F. Oulton, D. F. P. Pile, Y. Liu, and X. Zhang, "Scattering of surface plasmon polaritons at abrupt surface interfaces: Implications for nanoscale cavities," *Phys. Rev. B* **76**, 035408 (2007).
13. K. Tanaka, G. Burr, T. Grosjean, T. Maletzky, and U. Fischer, "Superfocussing in a metal-coated tetrahedral tip by dimensional reduction of surface-to edge-plasmon modes," *Appl. Phys. B* **93**, 257–266 (2008).
14. P. Berini, "Plasmon-polariton waves guided by thin lossy metal films of finite width: Bound modes of asymmetric structures," *Phys. Rev. B* **63**, 125417 (2001).

15. J. Grandidier, G. C. des Francs, L. Markey, A. Bouhelier, S. Massenot, J.-C. Weeber, and A. Dereux, "Dielectric-loaded surface plasmon polariton waveguides on a finite-width metal strip," *Appl. Phys. Lett.* **96**, 063105 (2010).
16. A. Bouhelier and G. P. Wiederrecht, "Excitation of broadband surface plasmon polaritons: Plasmonic continuum spectroscopy," *Phys. Rev. B* **71**, 195406 (2005).
17. A. Hohenau, J. R. Krenn, A. L. Stepanov, A. Drezet, H. Ditlbacher, B. Steinberger, A. Leitner, and F. R. Aussenegg, "Dielectric optical elements for surface plasmons," *Opt. Lett.* **30**, 893–895 (2005).
18. B. Hecht, H. Bielefeldt, L. Novotny, Y. Inouye, D. W. Pohl, "Local Excitation, Scattering, and Interference of Surface Plasmons," *Phys. Rev. Lett.* **77**, 1889 (1996).
19. A. Bouhelier and Th. Huser and H. Tamaru and H.-J. Güntherodt and D. W. Pohl and F. I. Baida and D. Van Labeke, "Plasmon optics of structured silver films," *Phys. Rev. B* **63**, 155404 (2001).
20. A. Drezet, A. Hohenau, D. Koller, A. Stepanov, H. Ditlbacher, B. Steinberger, F. Aussenegg, A. Leitner, and J. Krenn, "Leakage radiation microscopy of surface plasmon polaritons," *Mat. Sci. Eng. B* **149**, 220–229 (2008).
21. S. Massenot, J.-C. Weeber, A. Bouhelier, G. C. des Francs, J. Grandidier, L. Markey, and A. Dereux, "Differential method for modeling dielectric-loaded surface plasmon polariton waveguides," *Opt. Express* **16**, 17599–17608 (2008).
22. M. Neviere and E. Popov, *Light Propagation in Periodic Media: Differential Theory and Design* (CRC Press, 2002).
23. J.-C. Weeber, A. Bouhelier, G. Colas des Francs, L. Markey, and A. Dereux, "Submicrometer in-plane integrated surface plasmon cavities," *Nano Lett.* **7**, 1352–1359 (2007).
24. D. K. Gramotnev and D. F. P. Pile, "Single-mode subwavelength waveguide with channel plasmon-polaritons in triangular grooves on a metal surface," *Appl. Phys. Lett.* **85**, 6323–6325 (2004).
25. R. Zia, A. Chandran, and M. L. Brongersma, "Dielectric waveguide model for guided surface polaritons," *Opt. Lett.* **30**, 1473–1475 (2005).
26. L. Novotny, "Allowed and forbidden light in near-field optics. i. a single dipolar light source," *J. Opt. Soc. Am. A* **14**, 91–104 (1997).
27. G. I. Stegeman, N. E. Glass, A. A. Maradudin, T. P. Shen, and R. F. Wallis, "Fresnel relations for surface polaritons at interfaces," *Opt. Lett.* **8**, 626–628 (1983).
28. G. Colas des Francs, J. Grandidier, S. Massenot, A. Bouhelier, J.-C. Weeber, and A. Dereux, "Integrated plasmonic waveguides: A mode solver based on density of states formulation," *Phys. Rev. B* **80**, 115419 (2009).
29. A. Degiron and D. Smith, "Numerical simulations of long-range plasmons," *Opt. Express* **14**, 1611–1625 (2006).
30. T. Vary and P. Markos, "Propagation of surface plasmons through planar interface," *SPIE* **7353**, 73530K (2009).
31. S. Massenot, J. Grandidier, A. Bouhelier, G. C. des Francs, L. Markey, J.-C. Weeber, A. Dereux, J. Renger, M. U. González, and R. Quidant, "Polymer-metal waveguides characterization by fourier plane leakage radiation microscopy," *Appl. Phys. Lett.* **91**, 243102 (2007).

---

## 1. Introduction

Plasmonic metal structures are amongst the elementary constituents capable of confining electromagnetic radiation to deep sub-wavelength scale. In this context, geometrical singularities [1–5] and surface discontinuities [6, 7] are playing a major role at controlling the flow of surface plasmon polaritons (SPP) by imposing stringent boundary conditions. The understanding of SPP interaction with metal edges and contours is therefore of prime importance for designing superior plasmonic devices with limited losses. A simple case of a structural nonuniformity for a planar plasmonic component is an edge separating a metal region from a dielectric medium. This problem was theoretically described by Wallis and co-workers for an SPP impinging the edge at normal incidence [8]: depending on the dielectric environment, SPP can be efficiently radiated out of the end face. This was experimentally confirmed by Dawson *et al.* [9]. Edges are radiative scatterers and are consequently poor reflectors [10, 11]. More recently, Oulton and co-workers developed a robust formalism based on a scattering matrix formulation to compute this SPP scattering problem [12].

Interestingly however, very few studies focused on the interaction of surface plasmons propagating along a discontinuity. Yet, this is of fundamental interest to understand how SPPs are behaving in confined geometries capable of reducing the dimensionality of the excitation [13]. For an SPP parallel to an edge, Weeber *et al.* observed an oscillatory pattern at the boundary that was used to explain the formation of plasmonic modes in strip waveguides [6]. Plasmon modes in these finite-size Au structures was theoretically shown to interact strongly with edges [14]

probably contributing to the decaying propagation of SPP confined in narrow strips [15].

In this paper, we demonstrate that conical diffraction of an SPP by a planar structural discontinuity leads to the excitation of a one-dimensional (1D) evanescent wave. Although not being an eigen mode of the system, this particular wave needs to be taken into account to fully understand SPP interactions with surface boundaries. We analyze the wave-vector content of the 1D wave by Fourier plane imaging and show that it does not radiate in the superstrate. We interrogate the dimensionality of the wave, its polarization properties and dielectric sensitivity.

## 2. Sample fabrication

To conduct our experiment, we fabricated a 60nm-thick extended Au gold pad ( $120\ \mu\text{m} \times 50\ \mu\text{m}$ ). The interesting regions are the edges and the corners at the periphery of the pad. The gold pad was prepared by e-beam lithography. After developing the exposed PMMA resist, a 60nm gold layer was thermally evaporated in a vacuum chamber (pressure  $< 1 \times 10^{-7}$  mbar) at a constant rate of 0.1 nm/s. Finally the sample was then liftoff in a warm trichloroethylene solution. The gold pad obtained was imaged with a scanning electron beam microscope (SEM) and characterized with an atomic force microscope (AFM). Figure 1(a) displays an electron micrograph of the Au pad termination together with the coordinate system used in this manuscript. The direction of propagation of the surface plasmon is indicated by the white arrow and corresponds to the positive y-direction. Figure 1(b) shows a cross section of the gold edge obtained by AFM.

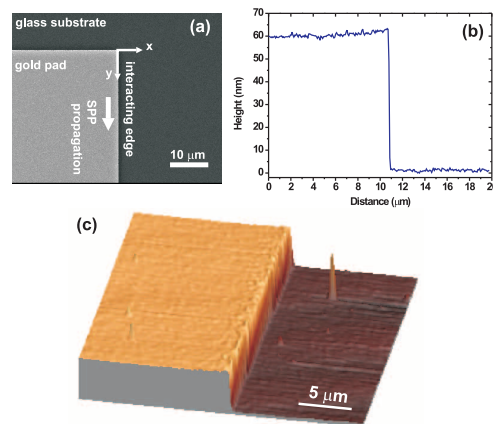


Fig. 1. (color online) (a) SEM image of the termination of a gold pad. The propagation direction of the surface plasmon is indicated by the arrow. (b) Cross section of the termination obtained by AFM. The height is 60nm. (c) Three dimensional rendering of the edge region characterized by AFM. The roughness of the gold film is estimated to be below 2nm RMS (small debris are visible in the edge vicinity).

The edge is clearly defined by an abrupt change of the height. The roughness of the gold film was measured at approximately 1.3nm root-mean-square (RMS). Figure 1(c) represents a three dimensional view of the terminated gold pad and its edge. Small debris are visible near the edge (up to a distance around  $1\ \mu\text{m}$ ) slightly increasing the roughness to 1.8nm RMS.

### 3. Experimental setup and differential method description

#### 3.1. Experimental setup

To measure the interaction of a surface plasmon and a  $90^\circ$  metal corner, We have developed a far-field excitation/detection schemes for exciting and characterizing surface plasmon running in metal surfaces. By use of high-numerical aperture (N.A.) objectives (N.A.=1.49), photons incident from the glass substrate have enough momentum to excite surface plasmons in a Kretschmann-like configuration illustrated in Fig. 2 [16, 17]. The position of a small collimated laser beam (diameter<1mm) is displaced from the optical axis of an inverted microscope (Nikon TE2000) to control the angle of incidence on the sample. The lateral displacement of the beam is chosen such the surface plasmon resonant angle ( $\sim 42^\circ$ ) is centered within the angular spread brought by the objective lens. The  $TM$ -polarization of the beam is adjusted by a combination of a polarizer and a half-wave plate. Detection of the surface plasmon propagation properties are determined by leakage radiation microscopy [18–20]. The sample is placed within the excitation spot by means of piezo-electrical actuators (Mad City Labs, NanoBio 100). Surface plasmon leakage radiations are directed to a beam splitter. Part of the beam is focused in the image plane of the microscope and provides a mapping of the surface plasmon intensity distribution in the film. An analyser placed in the path provides for a polarization-sensitive detection. The second part of the beam is passing a lens doublet that Fourier-transforms the signal. A camera placed at the conjugated Fourier plane renders the angular distribution of emitted light mapping thus the wavevector distribution  $k_x$  and  $k_y$ .

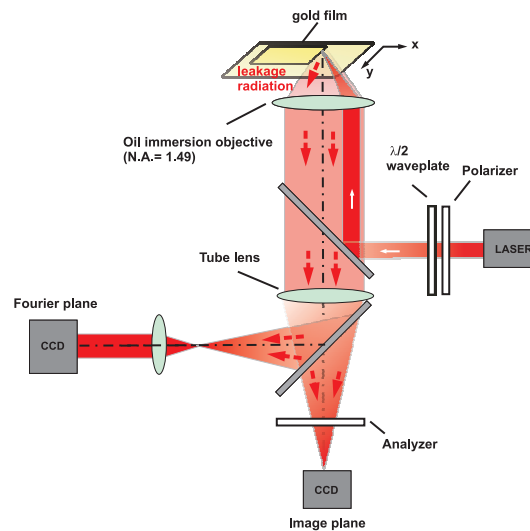


Fig. 2. (color online) Representation of the experimental setup. Surface plasmon are excited by a high N.A. objective in a Kretschmann-like configuration. Leakage radiation emitted in the substrate are collected by the same objective and detected by are directed on CCD cameras conjugated with either the image plane to retrieve the SPP intensity distribution, or with the Fourier plane to map the wavevector distribution.

#### 3.2. Differential method

The interaction of the surface plasmon with edge during propagation was computed using the Differential method which is a grating formalism based on Fourier expansion [21–23]. A schematic view of the geometry is illustrated in Fig. 3. The extended gold region is approx-

imated by a gold strip of  $10\ \mu\text{m}$  width and  $60\ \text{nm}$  tall. We assume in this condition that the characteristics of the SPP in this single strip is not different with a SPP on an extended gold film (identical wavevector and propagation length) [7].

The method separates the homogeneous areas (semi-infinite substrate and superstrate) from the modulated area (Au grating) where the fields are written in a Fourier expansion. The field in the superstrate (air) and the substrate (glass) can be expressed as a sum of plane waves (Rayleigh formalism). The differential method outputs the coefficients of the expansion from which the diffraction efficiencies of the periodic structure can be determined. In our approach, the grating efficiency is not the primary concern since we are interested at the diffraction by a single edge. Consequently, the periodicity between Au stripes is intentionally kept large at  $20\ \mu\text{m}$  to avoid any cross-talk between adjacent structures.

The excitation of surface plasmon in a single stripe is achieved by focussing a monochromatic three dimensional Gaussian beam. The finite-size excitation results from a plane wave decomposition of the Gaussian profile. The decomposition is restricted to a range of angles around the surface plasmon resonance. The azimuthal angle is adjusted for conical diffraction such that the on-axis projected component are aligned with the edge ( $y$ -direction). The total field is then computed in the  $(x, y)$  plane at an observation height corresponding to the thickness of the Au stripe ( $60\text{nm}$ ).

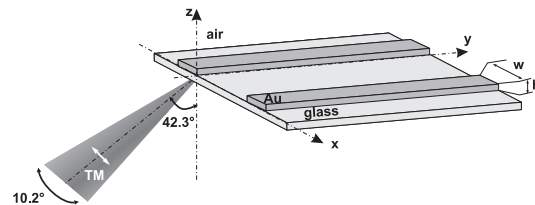


Fig. 3. Schematic view of sample geometry used for the computing the edge interaction with the differential method. The gold pads are approximated by  $w=10\ \mu\text{m}$  wide gold stripe with thickness  $h$  of  $60\text{nm}$ . The period of the stripe is  $20\ \mu\text{m}$ . A focused Gaussian beam is incident at the surface plasmon angle and is aligned with  $y$  axis.

#### 4. Results and discussion

The Au pad described above is installed on the experimental setup. The corner at the origin of the coordinate system is placed in the illumination area. Surface plasmon excitation is provided by the resonant illumination condition (angle) and momentum conversion brought by the corner (scattering). An image of the leakage intensity distribution is displayed in Fig. 4(a). The Au pad is delimited by the dashed line and appears as a darker region under a weak bright-field illumination. The upper right corner of the pad is located in  $(x; y) = (0; 0)$ . The excitation area is the intensity-saturated region in the image. Note that the maximum of the excitation area coincides with the edge and does not fully overlap the Au pad. The plane of incidence is aligned with the  $y$ -axis defining thus a plasmon propagation along  $y > 0$  as shown by the arrow in Fig. 4(a).

The interaction between the SPP and the discontinuity results in a large increase of the intensity at the edge as shown by the profile at bottom of Fig. 4(a). The shoulder at  $x = -2\ \mu\text{m}$  is assigned to the film's SPP.

To confirm our observations, we have simulated this edge interaction using the differential method. Figure 4(b) shows the computed electric field intensity at the metal/air interface for a situation mimicking Fig. 4(a). The incident beam is a three-dimensional focused Gaussian beam incident from the substrate at the SPP resonant angle with an azimuth aligned with the

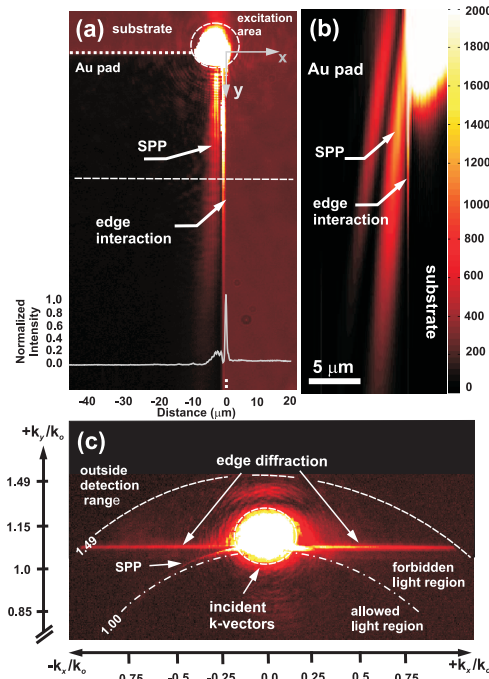


Fig. 4. (color online) (a) Intensity distribution of the SPP interaction with the edge acquired by leakage radiation microscopy. The excitation is visible as a saturated area on the top right corner of the Au pad. The SPP propagates towards  $y > 0$ . The intensity profile is taken at  $y = 34 \mu\text{m}$  (dashed line). (b) Simulation of the electric field intensity displaying the edge interaction. (c) Fourier imaging of the wave-vector content. The SPP is visible as a bright arc at  $k_{spp} = 1.04k_0$ . Its diffraction at the edge leads to a line with a constant  $k_y$ .

edge. In concord with our experimental results, SPP are visible on the Au pad concomitant of a high intensity localized at the edge [24, 25].

To gain more insight, we recorded the in-plane projection of the wave-vectors. Figure 4(c) displays a partial view of the Fourier plane limited to the reciprocal space of interest. The dashed-dotted line indicates the critical wave vector separating the allowed light region from the forbidden light region [26]. Above that line, light momentum is greater than in free-space and only evanescent waves can exist. The dotted line denotes our detection limit  $k_{max} = 1.49k_0$  imposed by our objective. The momentum spread of the focused excitation in Fig. 4(a) is contained within  $k_y = (1.1 \pm 0.15)k_0$  and  $k_x = \pm 0.25k_0$ . The wave-vectors associated with the SPP are recognized as a bright arc at  $k_{spp} = \sqrt{k_x^2 + k_y^2} = 1.04k_0$ . The arc is visible for  $k_x/k_0 < 0$ , because the SPP can only exist on metal surface, i.e.  $x < 0$ . The bright contrast of the arc is explained by the additional momentum obtained by scattering of the incident wave-vectors at the corner. Its brightness decays for negative  $k_x/k_0$ , because the polarization of the SPP is purely TM-polarized only for  $k_x/k_0 = 0$ .

The most interesting feature in Fig. 4(c) is undoubtedly the presence of an horizontal line at  $k_y = 1.04k_0$ . The line indicates the existence of a large spread of momentum along the  $k_x/k_0$  axis that spans the complete detection window ( $k_x = \pm 1.07k_0$ ) while being constant along the  $k_y/k_0$  axis at  $1.04k_0$ . The discontinuity being along the  $x$ -direction, a spread of wave-vectors is produced along the reciprocal axis. Because the wave-vector on the  $k_y/k_0$  axis corresponds to  $k_{spp}$ , we attribute this feature to conical diffraction of the SPP at the edge of the Au pad

under total internal reflection (TIR). The estimated critical angle for surface plasmon TIR at the Au/air interface is  $\arcsin(1/1.04) = 74^\circ$  [27], clearly below our grazing incidence.

A large distribution of momentum like the one observed along the  $k_x/k_o$  axis is the consequence of field confinement. In our case, the confinement is taking place at the edge as already eluded in Fig. 4(a). It is remarkable to note that this particular Fourier content is indicative of a one-dimensional (1D) excitation. The nature of a 1D wave imposes two wave-vector components to be imaginary [4]. This condition is confirmed in Fig. 4(c) as the momentum of the wave is entirely located in the forbidden-light region. This situation can be viewed as the surface plasmon equivalent of a laser beam incident on the hypotenuse of a glass prism at angle above the critical value. Under TIR, a three-dimensional beam creates a two-dimensional evanescent wave at the surface reducing thus the dimensionality of the field. We emphasized that the observed 1D wave is not an eigen mode of an edge but the result of conical diffraction of an SPP. Calculated effective indices of edge modes are beyond the detection window of our instrument [14].

We have confirmed that this particular Fourier signature is characteristic of a SPP running collinear to a metal edge. Diffraction under normal incidence (propagation along  $x$ ) only increases the incident spread of momentum along the  $k_y/k_o$  axis (data not shown).

The horizontal line observed in Fig. 4(c) has a finite width along the  $k_y/k_o$  axis. In a plasmonic waveguide, this line characterizes the mode sustained by the structure and its width is inversely proportional to its propagation length [28]. In our case, the width of the line contains information about the wave-vector content of the incoming SPP: when  $k_x$  components are present in the SPP momentum, the width of the line characterizing the 1D wave is increased. This situation is depicted in Fig. 5(a) showing the profile of the Fourier plane along the  $k_y/k_o$

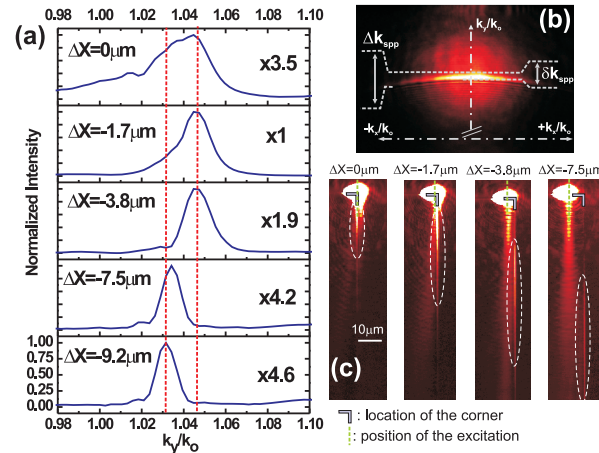


Fig. 5. (color online) (a) Profile of the wave-vector distribution along the  $k_y/k_o$  axis as a function  $\Delta x$ .  $\Delta x=0$  at the corner of the pad. (b) Wave-vector distribution showing  $k_{spp}$  when the excitation area is far from the edge.  $\Delta k_{spp}$  defines the complete SPP momentum spread of projected along the  $k_y/k_o$  axis.  $\delta k_{spp}$  is the FWHM of the SPP at  $k_x/k_o=0$ . (c) Leakage radiation images for the corresponding  $\Delta x$  values.

plotted for several lateral displacements  $\Delta x$  of the beam along  $x < 0$ . The value  $\Delta x=0 \mu\text{m}$  approximately coincides with an excitation area centered at the origin. Moving the beam laterally on the Au pad decreases the width of the Fourier line and shifts it to lower  $k_y/k_o$  values. This is accompanied by a reduction of the line intensity (multiplicative factors in Fig. 5(a)) indicating

a weaker interaction with the edge for increasing  $\Delta x$ . To understand this position-dependent width, let us consider the situation where the excitation area is located far away from the vertical edge. The SPP wave-vector content is displayed in Fig. 5(b). The SPP signature appears as a bright arc of circle of on-axis and off-axis wave-vector components superimposed over the non-resonant contributions of the illumination (homogeneous disk). The losses in the metal are responsible for the width  $\delta k_{spp}$  at  $k_x=0$ . Here  $\delta k_{spp}$  at full-width at half-maximum (FWHM) is equal to 0.011 and corresponds to  $k_{spp} = 1/(k_o \times \delta k_{spp}) = 11.3 \mu\text{m}$ . Using the intensity distribution of Fig. 4(a), we found that the exponential attenuation of the surface plasmon in the film is  $L_{spp} = 11.7 \pm 0.5 \mu\text{m}$  in agreement with the Fourier plane estimation. The attenuation along the edge is larger than  $L_{spp}$  with  $L_{edge} = 8.4 \pm 0.5 \mu\text{m}$ . We explain the shorter extension at the edge to the additional decay channel brought by the leakage of the 1D wave into the substrate and by the edge roughness induced by the fabrication process (Fig. 1(c)).

In Fig. 5(b),  $\Delta k_{spp}$  is the projection of all  $k_{spp}$  on the  $k_y/k_o$  axis contained within the incident wave-vectors spread ( $\Delta k_{spp}=0.036$ ). When the edge is present and  $\Delta x=0$ , the measured width of the Fourier line is 0.031. The corresponding intensity distribution of Fig. 5(c) shows a damped  $L_{edge}$ . Under this excitation condition, all  $k_{spp}$  (on and off-axis components) are sensing the discontinuity explaining thus why the measured line width is comparable to  $\Delta k_{spp}$ . As the edge leaves the excitation area ( $\Delta x < 0$ ), the line width decreases to reach 0.01, a value comparable to  $\delta k_{spp}$ . This narrowing suggests that a limited spread of wave-vectors is diffracted by the edge. We argue that, for  $\Delta x < 0$ , SPP propagation is filtering the interacting  $k_{spp}$  by selecting only those having  $k_x$  components. For  $k_{spp}$  with a non-zero  $k_x$  component, the  $k_y$  value must decrease since  $k_{spp} = \sqrt{k_x^2 + k_y^2}$ . This is confirmed by the displacement of the position of the line from  $1.046k_o$  at  $\Delta x = -1.7 \mu\text{m}$  to  $1.031k_o$  at  $\Delta x = -9.2 \mu\text{m}$  (Fig. 5(a)). Our argumentation is further supported by the displacement of the edge intensity along the y-direction indicating that different off-axis SPP components are being diffracted (dashed circles in Fig. 5(c)).

Because the field profile wraps around the discontinuity [14, 29], an electric field component normal to the edge must be present. Figure 6(a) shows a plot of the intensity taken at the edge as a function of the orientation of an analyser ( $A$ ) placed in the detection path. The analyser is collinear to the  $TM$  polarization at  $90^\circ$ . The intensity follows an expected sinusoidal dependence indicating that the largest field component is aligned with the edge. When  $A$  is collinear to the incident polarization  $P$ , the intensity distribution (Fig. 6(b)) resembles that of Fig. 4(a). However, when  $A$  is orthogonal, the intensity is reduced down to 15% but is not zero. Looking at the intensity distribution of Fig. 6(c), only the edge interaction is present in the image and the remaining  $TE$  component creating during focusing; the SPP contribution is completely suppressed under this analyzer orientation. We therefore conclude that there is a component normal to the discontinuity bearing similarities to the radial cylindrical mode of a nanowire. We have verified that this depolarization is characteristics of SPP conical diffraction. The intensity diffracted at an edge by an SPP incident along the normal vanishes completely when the polarizers are crossed (data not shown).

Finally, we interrogated the effect of a dielectric load on the edge interaction. Since the 1D wave is confined by the metal discontinuity, we anticipate a strong sensitivity when the local dielectric conditions are changed. To this aim, we evaporated a 24 nm-thick  $\text{SiO}_2$  layer on the Au pad at different recessed distances  $d$  from the edge as shown in the inset of Fig. 7. A completely covered edge corresponds to  $d = 0$ . In this situation, the film SPP is excited at the Au/ $\text{SiO}_2$  interface with  $k_{spp}^{\text{SiO}_2} = 1.1k_o$ . Upon diffraction by the edge, the 1D excitation retains the momentum of the incident SPP ( $k_y = 1.1k_o$ ) as observed in the Fourier profile (top panel of Fig. 7) and its corresponding illustration. For a recessed distance  $d=400$  nm, the  $k_y/k_o$  position of the 1D wave is not affected and remains at  $1.1k_o$ . This is unexpected since the edge is exposed to air. We interpret this results using the following argumentation. At a wavelength of 780 nm,

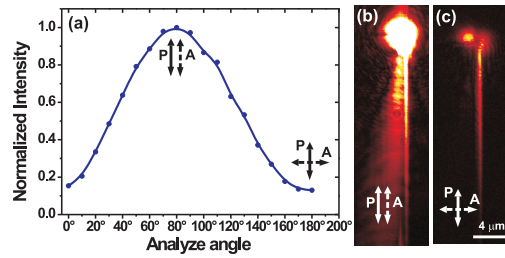


Fig. 6. (color online) (a) Normalized intensity of the edge diffraction as a function of the analyzing orientation. (b) and (c) are the intensity distributions of the edge diffraction for two orthogonal orientations of the analyzer.

the SPP mode sustained at a Au/air interface by a 400 nm-wide Au strip is below cutoff [6, 7]. Therefore, the only relevant mode excited in the structure is the one at the Au/SiO<sub>2</sub> at  $k_{spp}^{SiO_2}$ .

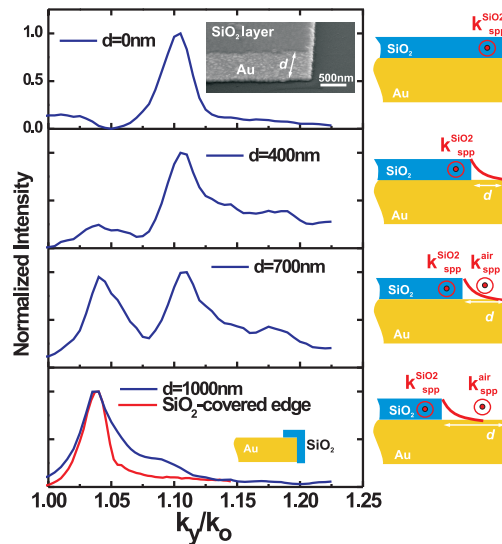


Fig. 7. (color online) Profile of the wave-vector distribution along the  $k_y/k_o$  axis for various recessed distances  $d$  and for a 100 nm-wide SiO<sub>2</sub>-covered edge (red curve) and their respective illustrations. Inset: Electron micrograph displaying the 24 nm-thick SiO<sub>2</sub> layer covering the Au pad and its recessed distance from the Au edge.

While this mode is essentially confined at the SiO<sub>2</sub> layer, its field must decay laterally on the air side of SiO<sub>2</sub>/air discontinuity [30]. Since the boundary condition imposes a conservation of the  $k_{spp}^{SiO_2}$  wave-vector, the edge is diffracting the decaying component along the  $x$  axis of the Au/SiO<sub>2</sub> SPP. As the distance  $d$  is increased, the SPP at the Au/Air interface can now exist with a momentum  $k_{spp}^{air}=1.04k_o$ . Because the excitation area is large compared to  $d$ , both SPP modes at  $k_{spp}^{air}$  and  $k_{spp}^{SiO_2}$  are excited simultaneously. This is the case for  $d=700$  nm. Remarkably, the corresponding profile in Fig. 7 shows that the edge can sustain two distinct 1D evanescent waves corresponding to the two SPP modes diffracted. By simply modifying the thickness of

the load, the momentum separation between these two waves can be adjusted. For  $d=1000$  nm, the laterally decaying contribution of  $k_{spp}^{SiO_2}$  is vanishing and the Fourier profile peaks at the  $k_{spp}^{air} = 1.04k_o$ . We confirmed this argumentation by covering the edge with 100 nm-wide SiO<sub>2</sub> strip, leaving the rest of the Au film exposed to air. Here too, the only relevant SPP is  $k_{spp}^{air}$  as the modes in the narrow SiO<sub>2</sub> strip are at cutoff. The wave-vector profile shown in the red curve at the bottom panel of Fig. 7 confirms that despite the dielectric load, the edge excitation retains the wave-vector of the Au/air SPP.

## 5. Conclusions

To summarize, we found that conical diffraction of a surface plasmon by a metal discontinuity under two-dimensional total internal reflection produces an excitation confined at the edge. By measuring its intensity and wave-vector distributions with leakage radiation microscopy, we demonstrate its one-dimensional evanescent character. We found that the dimensionality can be adjusted by the off-axis wave-vector spread of the incident SPP and its polarization has two in-plane components. We further demonstrate that an edge can simultaneously sustain distinct 1D waves separated in momentum space. Furthermore, we found that under certain condition, these waves are insensitive to the dielectric load of the edge. Although not being an eigen mode of the edge, the wave-vector and field profile characteristics of the 1D wave resembles that of a cylindrical mode of a metal nanowire. We believe that the existence of this SPP edge interaction has to be taken into account for designing plasmonic devices with optimal geometries. Finally, compared to plasmonic waveguide based on a dielectric load [31], the 1D wave offers an accessible non-radiative field localization at the edge that can be utilized for applications where large field gradients are required.

## Acknowledgment

The work was funded by NanoSci E+ program under grant E<sup>2</sup>-PLAS (ANR-08-NSCI-007).